applied sciences

MDPI

*Article*

# External Beam IBA Measurements for Cultural Heritage

**Massimo Chiari**

INFN Division of Florence, Via G. Sansone 1, I-50019 Sesto Fiorentino, Italy; chiari@fi.infn.it

**Abstract:** Ion beam analysis (IBA) methods refer to a set of analytical techniques based on the interactions of energetic ions, produced by a particle accelerator, with matter. The result of such interactions is the emission of characteristic radiation, X and gamma rays, and charged particles, which, upon detection, provide valuable information on the absolute concentration and depth distribution of the elements in the bombarded material. Moreover, IBA techniques can be performed while maintaining the object to be investigated at atmospheric pressure, without placing it in vacuum, in an analysis chamber, with the impinging ion beam extracted from the in-vacuum beamline of the accelerator, avoiding the need of invasive sampling and greatly easing the object positioning, thus allowing precious and big or large artefacts to be studied. This feature has opened the way for applications of IBA techniques for compositional analysis in cultural heritage studies, providing detailed and complete information about elemental compositions and depth distributions of analysed materials that are otherwise difficult or impossible for other analytical techniques. In this paper, the basic principles of the main IBA techniques applied to cultural heritage, namely, particle induced X-ray emission (PIXE), particle induced Gamma-ray emission (PIGE), and Rutherford or elastic backscattering spectrometry (RBS/EBS), will be recalled, and specific and practical details on how these techniques can be used for analysing cultural heritage objects with external beam set-ups will be provided.

**Keywords:** ion beam analysis; PIXE; PIGE; RBS; cultural heritage; external beam



**Citation:** Chiari, M. External Beam IBA Measurements for Cultural Heritage. *Appl. Sci.* **2023**, *13*, 3366. https://doi.org/10.3390/app13053366

Academic Editors: Maria Pia Riccardi, Daniela Di Martino and Massimiliano Clemenza

Received: 9 February 2023
Revised: 1 March 2023
Accepted: 3 March 2023
Published: 6 March 2023



## 1. Introduction

Nuclear physics has contributed for several decades to the cultural heritage field via a wide range of analytical methods to determine the composition or the age of an artifact, and it played a role in the conservation of art and archaeological objects. The availability of small and medium energy accelerator facilities has enabled an extensive use of analytical ion beam techniques to obtain information about archaeological and art objects: ion beam analysis (IBA) methods for compositional studies and accelerator mass spectrometry (AMS) for radiocarbon dating.

IBA are, generally, a suite of analytical techniques that exploit the interactions of rapid (~MeV energy) charged particles with matter to determine the elemental composition and structure of the surface regions of solids inferred from measured quantities such as the X-ray, gamma-ray, and charged particle spectra [1]. IBA are based on the interactions, at both the atomic and the nuclear level, between accelerated charged particles (ion beam) and the bombarded material. When a charged particle moving at high speed strikes a material, it interacts with the electrons and nuclei of the material atoms, gradually losing energy and slowing down. This interaction can lead to the emission of particles or radiation whose energy is characteristic of the elements that constitute the sample material. Moreover, the emission rates of those particles and radiation are proportional to the concentration of the emitting elements.

IBA share some common features: they are multi-elemental (all elements from H to U can be determined simultaneously), they allow quantitative analysis with high sensitivity (down to 1–100 ppm with experimental uncertainties in the few percent range), they are

non-destructive, and, in principle, do not require any sample extraction, preparation, or pre-treatment (thus, further measurements with other complementary techniques can be carried out). Although they probe only the surface of the material—the first tens of microns, depending on the range of the bombarding charged particles, that, in turn, depends on the type of matrix—they allow to obtain the depth profile of the elements. Ion beams can be focused using a system of magnetic quadrupole lenses (depending on the application it could be a doublet, a triplet or a quintuplet) to dimensions with sub-micron lateral resolution (nuclear microprobe) and microanalysis at some particular point or region can be performed. If the focused microbeam is scanned over the sample, or, conversely, the sample is moved in micrometric steps in the plane perpendicular to the microbeam direction, it is possible to obtain an imaging of the elemental spatial distribution.

IBA can contribute to cultural heritage studies [2], mainly by identifying the materials through the analysis of major elements, by helping in understanding the provenance of materials (sources of raw materials and trade routes) with the analysis of trace elements and by determining the manufacture technology thanks to the high spatial and depth resolutions achievable with these analytical techniques.

## 2. External Beam

IBA techniques are typically performed in a vacuum chamber, for instance, in material science applications, but they can easily be performed with an external beam, i.e., with the ion beam extracted from the vacuum beam line of the accelerator into ambient pressure through a thin extraction window typically glued to the end part (exit nozzle) of the vacuum—the line from the accelerator [3]. The window material and its thickness are chosen in order to guarantee first resistance to the pressure gradient and resistance under beam irradiation. The window has then to be thin enough not to affect too much the beam properties (energy and lateral resolution) and to produce negligible background radiation when traversed by the beam. Whereas in the past 7.5–8 μm thick polymeric films (Kapton, $C_{22}H_{10}N_2O_5$ or Upilex, $C_{22}H_{10}N_2O_4$), or thin metallic films (Al, Zr) in the few micrometres range where used, nowadays, 50–500 nm thick inorganic membranes ($Si_3N_4$) are typically employed (the thinner membranes are used for beam extraction on nuclear microprobes [4]). The object to be analysed is then placed typically at about 1 cm distance from the window, with the possibility of flooding this path with He, for reducing beam energy loss, energy straggling, and lateral spread. For instance, the effect on 3 MeV protons passing through a 100 nm or 500 nm thick $Si_3N_4$ membrane plus traversing in addition 1 cm of He before impinging on the sample, calculated with the SRIM-2008 code [5], is only an energy loss of 54 keV or 184 keV and an energy straggling of 6.4 keV or 12.4 keV, respectively.

Working with an external beam set-up, especially for cultural heritage studies, as in many ion beam laboratories [6–17], has the advantage of allowing fast and efficient measurements with direct analysis and easy positioning of object having any size and shape, without need of sampling, and no charging effects and heating from beam irradiation, thus strongly reducing the risk of damaging the object (truly "not deliberately destructive" measurements).

Evidently, working with an external beam set-up has limitations and drawbacks such as beam energy loss, beam energy straggling, as discussed above, and increased beam lateral spread, the latter one limiting the physical size of an extracted nuclear microprobe. In addition, to reduce the increased energy straggling caused when heavier ions are passing through the exit window and the path in atmosphere, external beam measurements are typically limited to the use of a proton ion beam. Moreover, a flow of He gas is needed to reduce also the attenuation of low-energy X-ray photons in the air.

In the following chapters, the basic principles of the principal IBA techniques applied to cultural heritage will be recalled, namely, particle induced X-ray emission (PIXE), particle induced Gamma-ray emission (PIGE), and Rutherford or elastic backscattering spectrometry (RBS/EBS), together with providing specific and practical details on

how these techniques can be used in analysing cultural heritage objects with external beam set-ups.

## 3. PIXE

In PIXE, an energetic beam of ions, usually protons, is directed towards the sample; as the ions cross the sample, they ionize the sample atoms, which emit characteristic X-rays, i.e., each atomic species emits X-rays with known energies. The minimum energy of detected X-rays is typically about 1 keV, thus all elements from Na to U are simultaneously detected; no information on organic elements (C, N and O) is obtained. Because X-rays do not lose energy as they cross the sample, but they can be eventually only attenuated, and they come from all the probed depth, PIXE determines total amounts of elements, not depth profiles. Among IBA techniques, PIXE is indeed unrivalled and the mostly used for the non-destructive analysis of cultural heritage objects [18] since it is highly sensitive over a broad range of elements, and it can be performed with external beams while maintaining the object in atmosphere. In this case, a He flow should be maintained in front of the X-ray detector to avoid attenuation of the low-energies X-rays in normal atmosphere, since 1 cm of air absorbs almost completely 1 keV X-rays, while the transmission is 99% in 1 cm of He. For the interpretation of PIXE spectra, the most used tool is the Guelph PIXE software package GUPIXWin v3.0.3 [19], widely applied and extensively tested in many publications through the use of certified reference materials.

Concerning the PIXE detector set-up, a more homogeneous efficiency and sensitivity over all the range of detected elements is achieved if a two-detectors set-up is adopted. These two detectors complement each other in terms of the efficiency curve and the covered solid angle, one dedicated to the low-Z element detection and the other to medium–high-Z element detection. This solution helps mitigating the intrinsic unbalance in the physics of X-ray production in PIXE, which favours the low- and medium-Z elements. This unbalance is a problem, for instance, when detecting low or trace quantities of high-Z elements in presence of a lower-Z matrix: if the count rate due to the low-energy X-rays emitted by low-Z elements is kept within tolerable limits, the total number of counts of X-rays from medium- and high-Z elements will result too small in reasonable measurement times. Thus, one detector is chosen with a large active area to cover the widest possible solid angle, thus increasing the detection efficiency regardless of the X-ray energy but is prevented from obtaining a large count rate from low-energy X-rays by shielding its surface with an absorber of appropriate thickness that absorbs the low-energy X-rays. This detector is thus optimized only for medium- and high-Z elements. The second detector, with no absorber and minimum dead layers, for instance, with a thin entrance window, but with a small active area and covering a much smaller solid angle, is then used to detect simultaneously the low energy X-ray emitted by the low-Z elements (Figure 1). Note that PIXE detectors with a thin entrance window used in presence of a large backscattered protons flux from the sample can suffer short-term effects and exhibit a worsening of the energy resolution under beam irradiation [20]. This quality loss of the acquired spectra is due to the deposit of MeV energy from the backscattered protons reaching the detector chip, leading to the saturation of the front-end electronics and to the increase of the noise level [21]. To divert these backscattered protons without substantial limitations to the detector intrinsic efficiency at low X-ray energies, a deflector made of permanent magnets is mounted in front of the detector. The use of a proton magnetic deflector is mandatory, for instance, in the ion beam analysis of aerosol particles samples collected on filters, where the ratio between total backscattered protons (from the filter) and X-rays (from aerosol particles) is typically about 1/10 or worse. In the analysis of cultural heritage objects, instead, the ratio between total backscattered protons and X-rays is typically about 1/100 or better, thus the short-term effects are negligible, and it is not crucial the installation of the proton divertor. Nevertheless, the use of a magnetic proton deflector in front of a PIXE detector, also in the case of cultural heritage applications, can avoid unrecoverable damages to the detector

chip from the long-term effects of backscattered proton irradiation, and the detector will last longer.

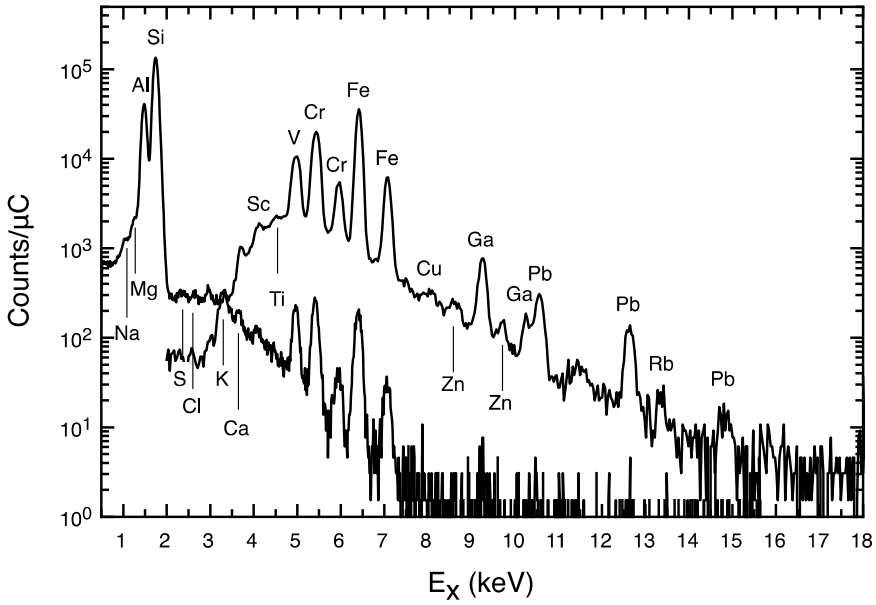


**Figure 1.** PIXE spectra of an emerald obtained with 3 MeV protons, collected simultaneously with a small area SDD for low-Z elements (Na-Ca) and a large area SDD with 450 mm Mylar foil as absorber for mid- and high-Z elements (Sc-Pb). The spectra are normalised by the proton beam charge accumulated during the measurement.

If only one detector is available, then the overall intensity between the high- and the low-energy region of the X-ray spectrum can be effectively balanced using a "funny filter" [22], i.e., an absorbing foil (typically Mylar, $C_{10}H_8O_4$) placed in front of the detector with a hole pierced so that a fraction of the X-ray within the detector solid angle is not attenuated. If the funny filter solution is adopted, it is advisable to choose a detector with a large active area (to increase the solid angle) and a thin entrance window (to enhance the transmission of low-energy X-rays).

With respect to the X-ray detectors, the PIXE analyst has currently two choices: traditional Lithium-drifted Silicon (Si(Li)) detectors that dominated PIXE set-ups up until a decade ago, or the new and unceasingly developing Silicon Drift Detectors (SDDs). The SDDs were first proposed in the early 1980s as a position-sensitive semiconductor detector for high energy charged particles, based on a novel charge transport scheme where the field responsible for the charge transport is independent of the depletion field [23], and they are now routinely employed in X-ray spectroscopy because of the low capacitance of the collecting electrode (0.5–1 pF/cm$^2$) and the low leakage current (1–2 nA/cm$^2$ at room temperature) resulting in improved energy resolution (<140 eV FHWM at Mn $K_\alpha$ line), yet at short shaping times (a few μs or less), thus allowing the sustaining of high count rates (up to 100 kHz), and just with a Peltier cooling element. The only drawback of SDDs is the limited thickness of the active region, typically 450–500 μm, although devices 1 mm or 2 mm thick are now available on the market, that reduce the intrinsic efficiency in the high-energy X-ray region, namely, above 20 keV. For instance, the intrinsic efficiency of a 450 μm thick SDD at 20 and 30 keV is about 37% and 14%, respectively, to be compared to values of about 99% and 81%, respectively, for a 5 mm thick Si(Li) detector [24]. However, this intrinsic inefficiency can be compensated by increasing the effective covered solid angle by installing an array of multiple identical SDDs in similar geometry and summing up offline the spectra from each, as implemented, for instance, in the external beam PIXE set-up of the New AGLAE accelerator in Paris, France [25], or by using a single large area SDD, with an active area much larger than typically achieved by traditional Si(Li), as

performed, for instance, in the external beam PIXE set-up of the INFN LABEC ion beam laboratory in Florence, Italy [26]. A comparison of the typical performances of a large area SDD and a Si(Li) for PIXE spectroscopy in the analysis of mid and high Z elements in a glass sample is shown in Figure 2.

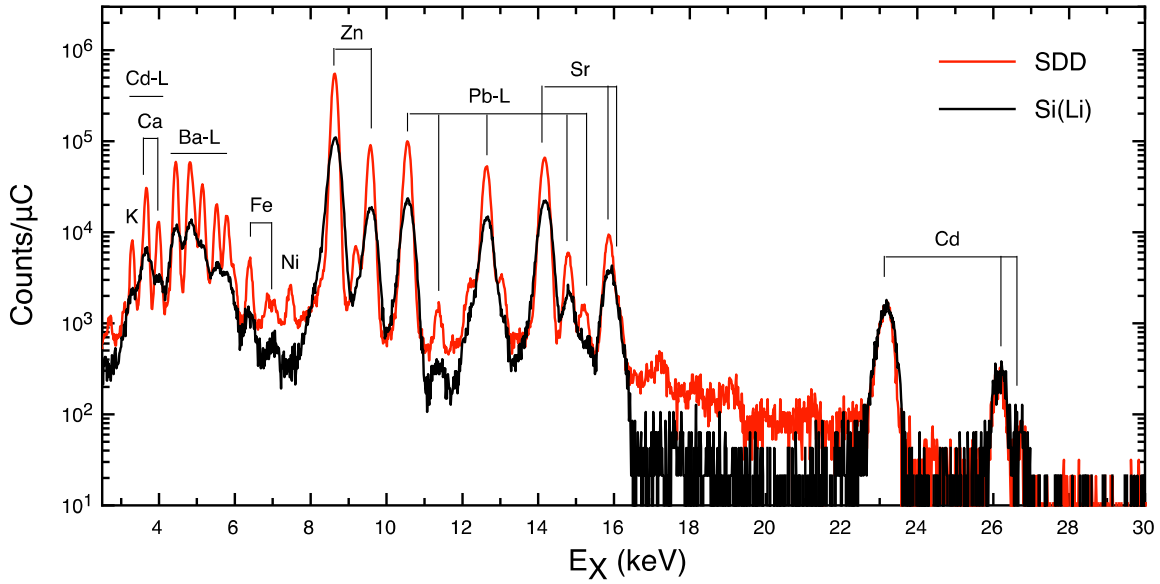


**Figure 2.** Comparison of PIXE spectra of a NIST 1412 glass obtained with 3 MeV protons, collected with a 150 $mm^2$, 450 μm thick SDD and with a traditional 80 $mm^2$, 5 mm thick Si(Li) detector. The spectra are normalised by the proton beam charge accumulated during the measurements.

*Differential PIXE*

Whereas PIXE does not provide elemental depth profiles, it is indeed possible to perform PIXE measurements in such a way that semi-quantitative information on stratigraphy in cultural heritage objects can be still obtained. The so-called "Differential PIXE" consists of performing point measurements on the same area with proton beams of different energies. At different beam energies, proton ranges, probed depths, and cross sections of X-ray production are different. Since the X-ray yields change as a function of the beam energy in a layered or heterogeneous in depth material depending mainly on the elemental distribution and the X-ray absorption in the material itself, by comparing PIXE spectra collected at different proton energies, stratigraphic information can be obtained, and, in layered objects, typical in cultural heritage, for example, paint layers [27], the sequence of layers can be inferred, although at a semi-quantitative level.

Operatively, for each measurement, first the apparent composition assuming a homogeneous matrix is obtained by analysing the PIXE spectra. If the material was legitimately homogeneous in depth, the ratios for the composition of the detected elements would be expected to be the same at different energies [28]. If not, the sample reveals a layered structure and if a composition ratio, for instance, element A-to-element B, increases (decreases) with increasing beam energy, this means that element A is present in a deeper (shallower) layer than element B. Moreover, when comparing two composition ratios, element A-to-element B and element C-to-element B and one ratio, for instance, element A-to-element B, increases more steeply than the other ratio, element C-to-element B, with increasing beam energy, then it means that element A is present in a deeper layer than element C.

As an example, we report here a differential PIXE analysis to reveal the stratigraphy of a tintype photograph. A selected homogeneous light-grey area of the tintype was investigated at three different proton energy: 2, 3, and 4 MeV in vacuum, corresponding to 1.91, 2.93, and 3.95 MeV on the sample surface, respectively (Figure 3, left panel). Several metallic elements were identified: Ti, Mn, Fe, Cr, Cu, Zn, and Ag. In case of a not-layered tintype, the same ratios of the concentrations of the main metallic elements would be

expected at different energies. With reference to the right panel of Figure 3, where only the elements Cr, Fe, Cu, Zn, and Ag are considered, practically the Cu-to-Ag and Cr-to-Ag composition ratios remain relatively constant at the different energies, showing that these elements could be either in the same layer or in contiguous thin layers, whereas both Zn-to-Ag and Fe-to-Ag composition ratios decrease with increasing beam energy, evidencing that Fe and Zn are present in a deeper layer than Ag. However, since the diminution of the Fe-to-Ag composition ratio has a steeper slope than the Zn-to-Ag one, it can be deduced that Fe is in a deeper layer than Zn. The semi-quantitative layered structure of the tintype revealed by differential PIXE measurements is Ag/(Ti, Mn, Cr, Cu)/Zn/Fe. The semi-quantitative approach proposed here is very easy to apply since it is based only on processing the PIXE spectra collected at different proton beam energies with the widespread GUPIXWin program and considering the departure of the calculated concentrations from those of a homogeneous sample as indication of a layered structure. Of course, compared to RBS/EBS, discussed in Section 5, it cannot provide quantitative results on the layer thickness and composition. Moreover, this simple differential PIXE approach typically fails when the same element appears in more than one layer.

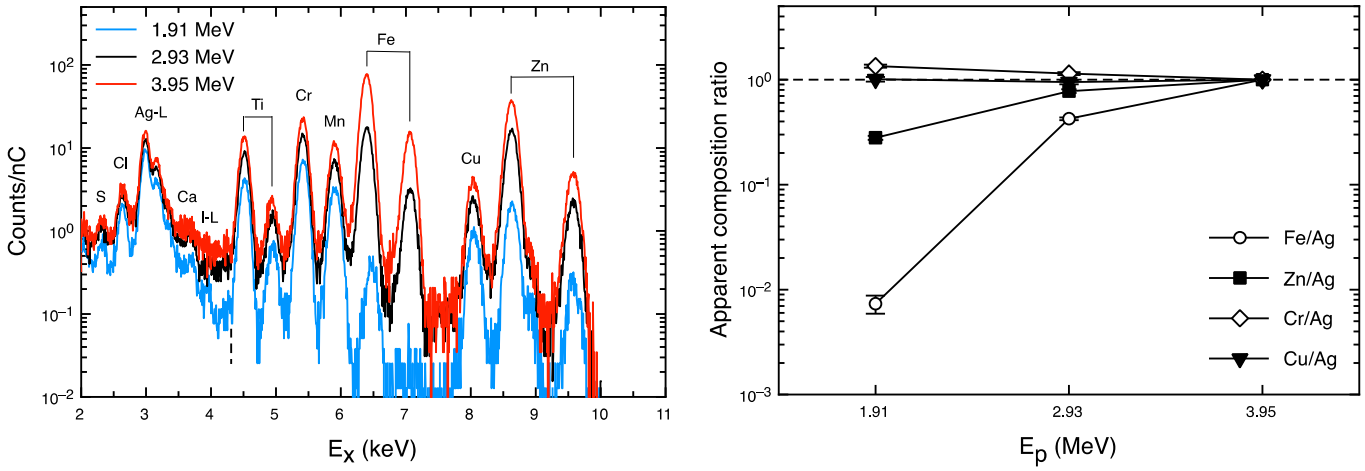


**Figure 3.** On the left, comparison between PIXE spectra of a tintype at three different proton energies, namely, 2, 3, and 4 MeV; the reported beam energies refer to the effective values at the sample surface, after traversing the beam exit window and about 1 cm path in external atmosphere. The spectra are normalised by the proton beam charge accumulated during the measurements. On the right, the apparent composition ratios of the main metallic elements as a function of the different proton beam energies.

## 4. PIGE

In PIGE, when the energetic beam of ions strikes the sample, if the ion beam energy is enough, it can lead to a nuclear reaction with a sample nucleus. In some cases, a characteristic gamma-ray is promptly emitted. The reactions occur only for certain beam species (typically, protons) and sample isotopes (usually light elements, i.e., Li, Be, B, F, Na); this means that PIGE is highly specific to given isotopes. Because emitted gamma rays do not lose energy as they cross the sample, and they come from all the probed depth, PIGE also determines total amounts, not depth profiles. The typical reactions induced by protons and the energy of characteristic gamma rays used for PIGE analysis of light elements for cultural heritage studies are shown in Table 1.

Given the high energy of the detected radiation, orders of magnitude higher than characteristic X-ray energy, the problem of absorption of the emitted radiation in the atmosphere in an external beam set-up is thus negligible, and the distance at which the PIGE detector is placed is not an issue, except for trying to maximise the subtended solid angle, hence the detection efficiency. The elements detected by PIGE are limited in number, but complementary to those detected by PIXE: in such a way PIGE technique is thus a

perfect "sidekick" or a companion of PIXE for the analysis of light elements in cultural heritage samples (Figure 4). Quantitative information from PIGE spectra is typically obtained by comparing the gamma-ray yields from the sample to those from homologous reference standards, although free dedicated codes for standard-less PIGE analysis, such as PIGRECO [29] and ERYA [30], are now becoming available.

**Table 1.** Main PIGE reactions induced by protons of interest for elemental analysis in cultural heritage.

| Element | Reaction | Gamma-Ray Energy (keV) | Isotopic Abundance |
|---|---|---|---|
| Li | $^{7}$Li(p,p′γ)$^{7}$Li | 478 | 92.4% |
| Be | $^{9}$Be(p,αγ)$^{6}$Li | 3562 | 100% |
| B | $^{10}$B(p,αγ)$^{7}$Be | 429 | 19.9% |
| F | $^{19}$F(p,p′γ)$^{19}$F<br>$^{19}$F(p,p′γ)$^{19}$F | 110<br>197 | 100%<br>100% |
| Na | $^{23}$Na(p,p′γ)$^{23}$Na | 441 | 100% |
| Mg | $^{25}$Mg(p,p′γ)$^{25}$Mg | 585 | 10.13% |
| Al | $^{27}$Al(p,p′γ)$^{27}$Al<br>$^{27}$Al(p,p′γ)$^{27}$Al | 843<br>1013 | 100%<br>100% |
| Si | $^{28}$Si(p,p′γ)$^{28}$Si<br>$^{29}$Si(p,p′γ)$^{29}$Si | 1779<br>1273 | 92.23%<br>4.67% |

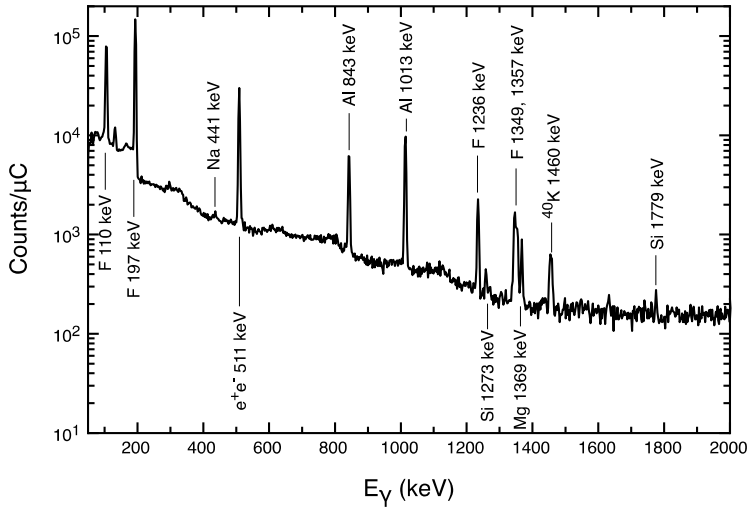


**Figure 4.** PIGE spectrum of a topaz obtained with 3 MeV protons, showing gamma-ray lines of F, Na, Al, Mg, and Si. The spectrum is normalised by the proton beam charge accumulated during the measurement.

The detectors typically employed for PIGE analysis are High-Purity Germanium (HPGe) detectors, because germanium is still the only material which can provide a combination of high-energy resolution and high-detection efficiency at the gamma-ray energy of interest. The drawback to using these detectors, though, has always been the need to cool them to cryogenic temperatures (about 77 K), using, traditionally, liquid nitrogen with a combination of a cryostat and a dewar. However, the modern electro-mechanical methods of achieving cryogenic temperatures have overcome the limits in convenience, practicality, and sustainability of a liquid-nitrogen-cooled device [31]. It has to be noted that less-expensive, compact, and lightweight inorganic scintillators such as Cerium-activated Lanthanum Bromide ($LaBr_3$(Cr)) detectors have been used as well for PIGE, although the achieved energy resolution is about one order of magnitude worse.

The benefit of PIXE-PIGE synergy can be elucidated in two case studies from the literature, namely, the identification of lapis lazuli pigment in paint layers [32] and the

quantification of sodium in ancient glasses [33,34]. Lapis lazuli is a blue pigment mainly composed of lazurite ($3Na_2O{\cdot}3Al_2O_3{\cdot}6SiO_2{\cdot}2Na_2S$). It was used since the Middle Ages in different painting techniques, and it was considered a very precious and expensive pigment. PIGE can be used to identify lapis lazuli in pigment layers using its Na component as a tracer by simply detecting the 441 keV gamma ray from the $^{23}Na(p,p'\gamma)^{23}Na$ reaction. On the contrary, PIXE is severely hampered in the possibility of identifying lapis lazuli in canvas and wood paintings, since the low energy X-rays emitted by the lighter characteristic elements (not only Na, but also Al and Si) are absorbed in the protective varnish layer and within the paint layer itself, especially when lapis lazuli is mixed with another a high-Z pigment, such as lead white. Moreover, in this case, the X-rays emitted by the highest Z element of lazurite (S), less affected by the aforementioned absorption problems, might be difficult to identify due to the overlap of Pb and S X-ray lines, even with the good energy resolution of SDDs. Detection and quantification of Na is crucial also in ancient glass studies to distinguish, for instance, the natron glass of the Roman times (with high $Na_2O$, and low $K_2O$ and MgO content) from later glass such as plant ash glass (with low $Na_2O$ and high $K_2O$ content), used since the Middle Ages. Unfortunately, a PIXE analysis could be completely blind to the presence of Na in the bulk of a sample, since the surface altered and corroded layers may strongly absorb the X-rays from the lightest elements (the 1 keV X-rays of Na are absorbed in the first few microns from the surface). A complementary use of PIXE and PIGE is particularly effective to address this problem: the PIGE analysis of Na, based on the integrated yield of the 441 keV gamma ray, refers to a much larger depth, since gamma rays are detected with negligible attenuation regardless of the depth from where they were originated. It is thus possible to immediately distinguish between surface and bulk Na composition from PIXE and PIGE measurements, respectively.

## 5. RBS/EBS

In RBS, an energetic beam of ions, usually protons or alpha particles, is directed towards the sample. As it hits a sample nucleus head-on, it is scattered back: the energy of the backscattered ions depends on the sample atomic species; thus, measuring it the sample atomic species is determined. All elements with an atomic mass A higher than the atomic mass of the ion beam are detected. Thus, for instance, by using a proton beam, all the elements heavier than protons (from deuterons on) can be detected. If there is more than one element in the sample, for instance, two, for simplicity, then two separate signals are observed: the heavier the sample atom, the higher the backscattered energy. As the ion beam crosses the sample, it slowly loses energy: ions which are backscattered at a certain depth arrive to the detector with lower energy than if they were backscattered at the surface, hence the energy scale can be transformed into a depth scale. The backscattered particle spectra can then simultaneously provide information on elemental composition, depth distributions, and on sample thickness. Since the mass resolution degrades as the ratio of the target nuclei mass to the ion beam mass increases, in particular, when a proton beam is used, RBS can be used efficiently to determine those light elements such as C, N, and O that are difficult or impossible to determine using PIXE or PIGE (Figure 5). RBS is often referred to also as EBS, since EBS is the natural extension of RBS for higher ion beam energies when the elastic scattering cross section cannot be considered purely Rutherford anymore [35]; when using protons as bombarding ion beams, as typical in cultural heritage IBA applications, this condition holds true for elastic backscattering on nuclei up to Zn when the proton energy is 3 MeV. Of course, the availability of experimental or theoretically evaluated elastic scattering cross sections for few MeV energy protons on such elements [36] is mandatory for the practical applicability of EBS. Quantitative information from RBS or EBS spectra are obtained from the results of simulation of the experimental spectra using dedicated codes, one of the widely used being SIMNRA [37].

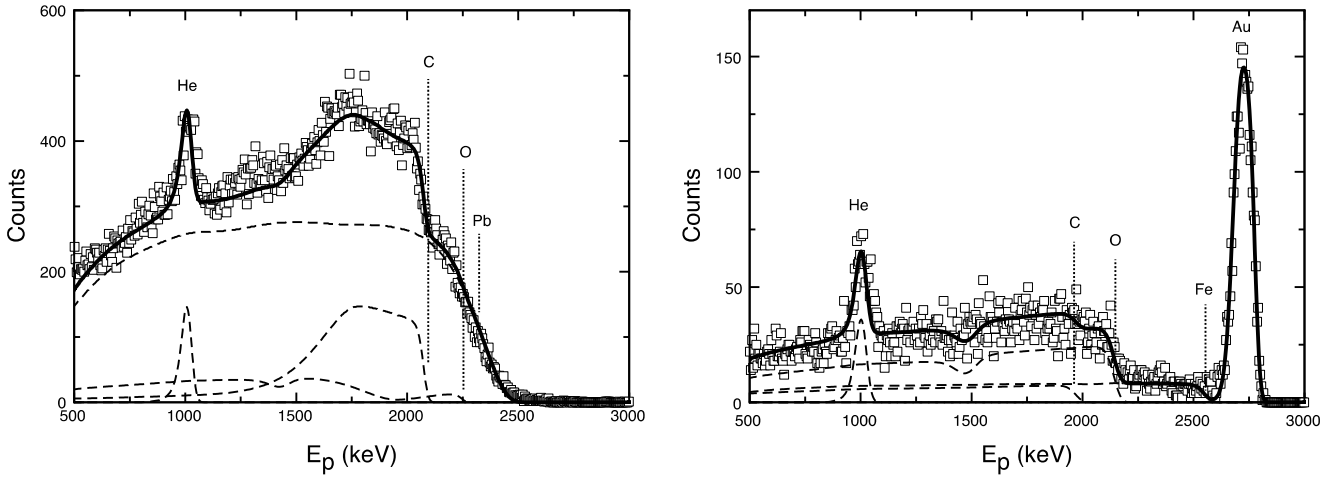


**Figure 5.** Experimental (open squares) and simulated (full line) RBS spectra obtained with 3 MeV protons. On the left, lead-white paint layer covered with about 15 µm thick varnish. On the right, 525 nm thick gold leaf laid on wood by a bole clay. The partial spectra of the detected elements (C, O, Fe, Pb, and Au), and the contribution of He from the helium flowing are shown as dashed lines.

It has to be noted that some of the intrinsic limitations when working with extracted beams, such as increased beam energy straggling and lateral spread, are making external beam RBS analysis less attractive than in an in-vacuum set-up, because these could worsen spectroscopic characteristics such as mass and depth resolution. The use of a He flow is thus welcomed also in this case, as is external beam PIXE, to mitigate these effects. Working under a helium flow produces a very distinctive feature in the particle spectra from external-beam RBS measurements, namely, the appearance of a peak due to elastic scattering of protons on He that does not belong to the sample itself, but it is a "parasitic" element, contained in the first layer that the protons encounter before interacting with the sample.

A proper design of the external beam RBS detection system can further reduce beam energy straggling and lateral spread effects. The charged particle detector, typically a Silicon surface barrier detector or a Si PIN diode, can be placed, for instance, inside a long aluminium case, maintained at a pressure of at least below 1 mbar (accomplished by a low vacuum pump such as a membrane pump) and closed at the end facing the incoming backscattered ions by a very thin window (a few µm thick Mylar foil or a few hundreds of nm thick silicon nitride membrane). In this way, the detector can be kept at the proper distance from the sample. The longer the distance the better the definition of the scattering angle and the less the angular spread, at the same time reducing the path that the backscattered ions have to travel in atmosphere at ambient pressure. In Table 2, the total energy resolution FWHM, achievable in external beam RBS with 3 MeV protons, is shown, including partial contributions to the total energy resolution due to the different elements in the set-up, starting from a detector with an energy resolution of 13 keV FWHM.

The values in Table 2 refer to two different ideal set-ups, using extracted standard, millimetre-sized beams or microbeams. The ultra-thin window for beam extraction and the short external path covered by the beam particles typically adopted in external microbeams allow obtaining a final total energy resolution for the external microbeam RBS system not very different from the in-vacuum RBS case, where only the detector energy resolution would contribute, whereas, in external standard millibeams, the achieved energy resolution is about 50% worse. Nonetheless, the obtained energy resolution values still allow valuable standard external RBS measurements, in particular, for light elements such as C, N, and O, which are difficult or impossible to determine with PIXE or PIGE.

**Table 2.** Total energy resolution FWHM, achievable in external beam RBS with 3 MeV protons, according to two different ideal set-ups, namely, using extracted standard or millimetre-sized beams and microbeams. The partial contributions to the total energy resolution, apart from detector energy resolution, due to the different main elements in the set-ups, calculated with the SRIM-2008 code [5], are indicated.

| | External Millibeam | | External Microbeam | |
|---|---|---|---|---|
| | **Thickness** | **Energy Straggling** | **Thickness** | **Energy Straggling** |
| Extraction window, $Si_3N_4$ | 500 nm | 7 keV | 100 nm | 3 keV |
| Window-sample path, He | 10 mm | 8 keV | 3 mm | 4 keV |
| Sample-detector path, He | 10 mm | 8 keV | 3 mm | 4 keV |
| Detector case window, Mylar | 1 μm | 7 keV | 1 μm | 7 keV |
| Detector dead-layer, Si | 310 nm | 5 keV | 310 nm | 5 keV |
| Detector energy resolution | | 13 keV | | 13 keV |
| Total energy resolution | | 21 keV | | 16 keV |

Spectra from simultaneous RBS and PIXE measurements are, nevertheless, often analysed separately to obtain complementary information, for instance, using RBS to obtain the composition of a low-Z matrix as input data for PIXE analysis of trace metals in that matrix [38]. In samples with a layered structure particle and X-ray spectra from PIXE and RBS, measurements can indeed be handled and analysed self-consistently and their synergic use permits to derive detailed data about composition and elemental depth distribution of the analysed material [39]. This approach is often referred to as "Total IBA" [40] or "Global IBA" [41]. As an example, we report here on external beam EBS-PIXE analysis of a presumed oil gilding on brass sample using a 3 MeV proton beam (Figure 6).

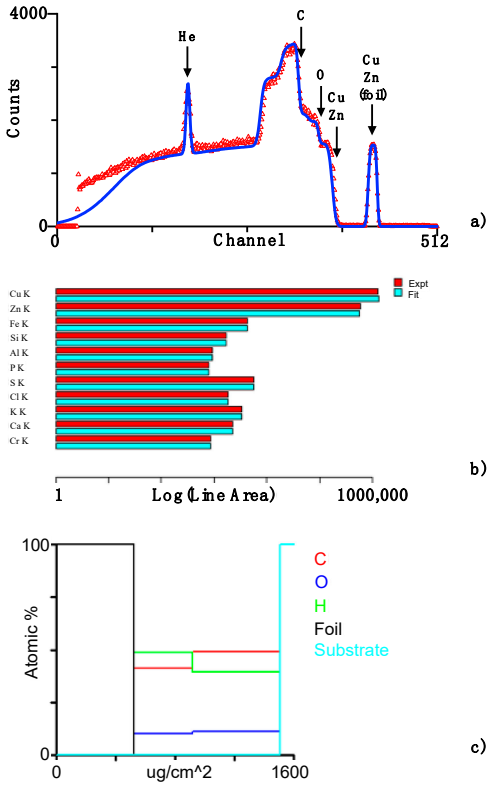


**Figure 6.** External beam IBA measurements of a presumed oil gilding on brass with 3 MeV protons. (**a**) Experimental (red symbols) and simulated (blue line) EBS spectra. (**b**) Comparison of experimental (red) and fitted (light blue) X-ray peak areas from PIXE, for main and trace elements. (**c**) Fitted structure of the sample showing the elemental depth distribution.

The EBS and PIXE spectra were analysed and fitted in a self-consistent approach using the DataFurnace code [42,43], and the sample actually revealed to be a thin copper foil as "gilding" (Cu 94% Zn 2% Fe 1%, 510 μg/cm$^2$ thick) applied with an oil-based size or mordant (H 40–49% C 41–49% O 10–11%, 1.0 mg/cm$^2$) on brass substrate (Cu 65% Zn 35%). It has to be noted that the simple differential PIXE semi-quantitative approach proposed here could not have easily resolved this stratigraphy, since the two elements Cu and Zn appear in more than one layer.

## 6. Beam Charge Measurements in External Set-Ups

Quantitative analysis with IBA techniques relies on the accurate knowledge of the number of beam ions striking the sample. This can be normally accomplished by measuring the collected beam charge, integrating the beam electrical current during the measurements. When dealing with cultural heritage objects this cannot be achieved simply in a direct way, since most objects are insulating materials and, moreover, their thickness is such to completely stop the ion beam and to prevent the use of a Faraday cup simply installed behind the sample. Thus, indirect ways, based on the measurement of some effect induced by the incoming ion beam, and depending on its intensity, have to be used to normalise X-ray, gamma-ray, and particle yields during the measurements.

Since the ion beam has to traverse an extraction window in external beam IBA measurements, the products of the interaction of the ions with the window material can be used profitably. The number of the beam particles impinging on the object to be analysed can then be measured indirectly by counting the number of Si X-rays produced by the beam in a $Si_3N_4$ extraction window [44] or, alternatively, by counting the number of backscattered beam particles from Si and N in the extraction window (Figure 7) [45]. The method based on backscattered beam particles can be applied also if the extraction window is a polymeric material made of C, N, O, and H, such as Kapton or Upilex, since no detectable X-ray would be emitted.

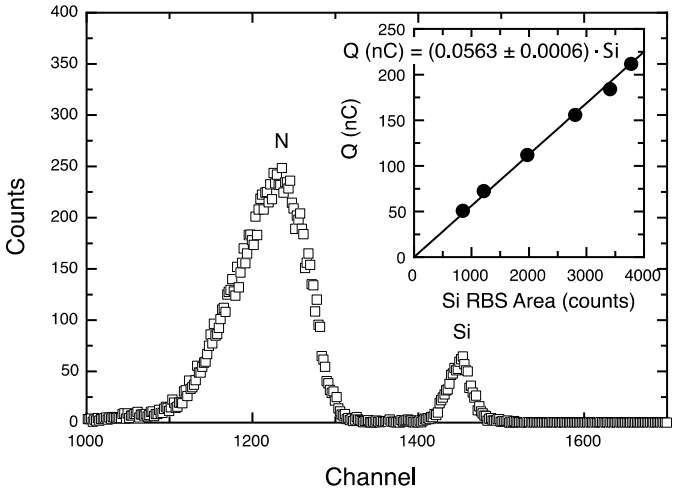


**Figure 7.** RBS spectrum of 2.5 MeV protons backscattered from Si and N in a 500 nm thick silicon nitride extraction window for beam normalization purposes. In the inset, a correlation between the area of the Si RBS peak and the integrated beam charge.

The beam charge deposited on the sample can be determined also using a beam chopper that periodically intersects the beam and samples its intensity, being either an in-vacuum system, for instance, measuring the Au RBS yield from rotating gold plated carbon blades placed before the exit nozzle [46], or an in-air system, for instance, measuring the Ni X-ray yield from a graphite vane covered with a thin nickel layer placed in the space between the extraction window and the sample [47].

It has to be noted that all these beam normalization methods rely on the installation and use of a dedicated detector, either an X-ray or a charged particle detector, followed also by its electronic data acquisition chain, thus a non-negligible investment is to be foreseen.

Alternatively, the peak from elastic backscattering of protons on He when working under a helium flow (see Figures 5 and 6), or the peak area of the X-rays from the Ar present in air in in-air PIXE systems [48], can be used as normalization, but this is not as robust as the aforementioned methods. Actually, the number of Helium nuclei or Argon atoms encountered before the protons interact with the sample depends upon the surface topography, the surface roughness of the sample, and on accurate reproducible positioning of the sample at the same distance from the extraction window from one measurement to the other.

## 7. Conclusions

External beam IBA techniques are still essential and important for compositional studies in cultural heritage because they can provide information about elemental surface and in-depth distribution in a non-invasive, non-damaging, and non-deliberatively destructing way. However, IBA techniques are based on the use of a large-footprint instrumentation, a particle accelerator, thus the impact of laboratory-based analytical techniques in those applications, such as cultural heritage, where the vast majority of the world cultural heritage is immovable could diminish in favour of increasingly more performing portable or transportable energy-dispersive X-ray fluorescence (ED-XRF) systems for elemental analysis and imaging of cultural heritage objects [49]. Nonetheless, ED-XRF is particularly sensitive for mid and high-Z alone, while IBA techniques demonstrate a high sensitivity to elements from all the periodic table, in particular, light elements that are not easily measurable and quantifiable using many analytical methods, allowing single measurement problems to be solved in ways that are otherwise difficult or impossible for other analytical techniques. Moreover, until now, any portable and/or transportable equipment does not offer the same performances as IBA with respect to the detection limits. In this regard, the development of smaller, compact, and transportable accelerators that will allow in situ IBA of cultural heritage materials, such as MACHINA, the Movable Accelerator for Cultural Heritage In situ Non-destructive Analysis [50], jointly developed by INFN, CERN, and the Opificio delle Pietre Dure (OPD), an Italian institute for the conservation of works of art, will pave the way to IBA measurements performed directly inside museums and conservation centres, to go where no accelerator has gone before.

**Funding:** This research received no external funding.

**Institutional Review Board Statement:** Not applicable.

**Informed Consent Statement:** Not applicable.

**Data Availability Statement:** The data presented in this study are available on request from the corresponding author.

**Acknowledgments:** The support of the scientific and technical staff at INFN LABEC ion beam laboratory is warmly acknowledged. The author wishes to thank the many colleagues and friends engaged in interesting discussions on the analysis of cultural heritage objects with ion beam techniques, during conferences, meetings, workshops, and visits. Special thanks to Chris Jeynes from the University of Surrey for his invaluable support in using the DataFurnace code.

**Conflicts of Interest:** The author declares no conflict of interest.

## References

1. Nastasi, M.; Mayer, J.; Wang, Y. *Ion Beam Analysis—Fundamentals and Applications*; CRC Press: Boca Raton, FL, USA, 2014.
2. Dran, J.; Salomon, J.; Calligaro, T.; Philippe, W. Ion beam analysis of art works: 14 years of use in the Louvre. *Nucl. Instrum. Methods B* **2004**, *219*, 7. [CrossRef]
3. Katsanos, A.; Xenoulis, A.; Hadjiantoniou, A.; Fink, R. An external beam technique for proton-induced X-ray emission analysis. *Nucl. Instrum. Methods* **1976**, *137*, 119. [CrossRef]

4. Giuntini, L. A review of external microbeams for ion beam analyses. *Anal. Bioanal. Chem.* **2011**, *401*, 785. [CrossRef] [PubMed]
5. Ziegler, J.; Ziegler, M.; Biersack, J. SRIM—The stopping and range of ions in matter (2010). *Nucl. Instrum. Methods B* **2010**, *268*, 1818. [CrossRef]
6. Ontalba-Salamanca, M.A.; Ager, F.; Ynsa, M.; Gomez-Tubio, B.; Respaldiza, M.; Garcia-Lopez, J.; Fernandez-Gomez, F.; de la Bandera, M.; Grime, G. External microbeam set-up at the CNA (Sevilla) and its application to the study of Tartesic jewellery. *Nucl. Instrum. Methods B* **2001**, *181*, 664. [CrossRef]
7. Šmit, Ž.; Fajfar, H.; Jeršek, M.; Knific, T.; Lux, J. Analysis of garnets from the archaeological sites in Slovenia. *Nucl. Instrum. Methods B* **2014**, *328*, 89. [CrossRef]
8. Sokaras, D.; Bistekos, E.; Georgiou, L.; Salomon, J.; Bogovac, M.; Aloupi-Siotis, E.; Paschalis, V.; Aslani, I.; Karabagia, S.; Lagoyannis, A.; et al. The new external ion beam analysis setup at the Demokritos Tandem accelerator and first applications in cultural heritage. *Nucl. Instrum. Methods B* **2011**, *269*, 519. [CrossRef]
9. Török, Z.; Huszánk, R.; Csedreki, L.; Dani, J.; Szoboszlai, Z.; Kertész, Z. Development of a new in-air micro-PIXE set-up with in-vacuum charge measurements in Atomki. *Nucl. Instrum. Methods B* **2015**, *362*, 167. [CrossRef]
10. Zucchiatti, A.; Climent-Font, A.; Gutierrez-Neira, P.C.; Perea, A.; Fernandez-Esquivel, P.; Rovira-Llorens, S.; Ruvalcaba-Sil, J.L.; Verde, A. Prehispanic goldwork technology study by PIXE analysis. *Nucl. Instrum. Methods B* **2014**, *332*, 160. [CrossRef]
11. Corregidor, V.; Oliveira, A.; Rodrigues, P.; Alves, L. Paintings on copper by the Flemish artist Frans Francken II: PIXEcharacterization by external microbeam. *Nucl. Instrum. Methods B* **2015**, *348*, 291. [CrossRef]
12. Ontalba-Salamanca, M.A.; Ruvalcaba-Sil, J.L.; Bucio, L.; Manzanilla, L.; Miranda, J. Ion beam analysis of pottery from Teotihuacan, Mexico. *Nucl. Instrum. Methods B* **2000**, *161–163*, 762. [CrossRef]
13. Demortier, G.; Fernandez-Gomez, F.; Ontalba-Salamanca, M.; Coquay, P. PIXE in an external microbeam arrangement for the study of finely decorated tartesic gold jewellery items. *Nucl. Instrum. Methods B* **1999**, *158*, 275. [CrossRef]
14. Mathis, F.; Othmane, G.; Vrielynck, O.; Calvo-del Castillo, H.; Chêne, G.; Dupuis, T.; Strivay, D. Combined PIXE/PIGE and IBIL with external beam applied to the analysis of Merovingian glass beads. *Nucl. Instrum. Methods B* **2010**, *268*, 2078. [CrossRef]
15. Santos, H.; Added, N.; Silva, T.; Rodrigues, C. External-RBS, PIXE and NRA analysis for ancient swords. *Nucl. Instrum. Methods B* **2015**, *345*, 42. [CrossRef]
16. Vadrucci, M.; Mazzinghi, A.; Gorghinian, A.; Picardi, L.; Ronsivalle, C.; Ruberto, C.; Chiari, M. Analysis of Roman Imperial coins by combined PIXE, HE-PIXE and μ-XRF. *Apple. Rad. Isot.* **2019**, *143*, 35. [CrossRef]
17. Beck, L.; Alloin, E.; Vigneron, A.; Caffy, I.; Klein, U. Ion beam analysis and AMS dating of the silver coin hoard of Preuschdorf (Alsace, France). *Nucl. Instrum. Methods B* **2017**, *406*, 93. [CrossRef]
18. Calligaro, T.; Gonzales, V.; Pichon, L. PIXE analysis of historical paintings: Is the gain worth the risk? *Nucl. Instrum. Methods B* **2015**, *363*, 135. [CrossRef]
19. Campbell, J.; Cureatz, D.; Flannigan, E.; Heirwegh, C.; Maxwell, J.; Russell, J.; Taylor, S. The Guelph PIXE Software Package V. *Nucl. Instrum. Methods B* **2021**, *499*, 77. [CrossRef]
20. Calzolai, G.; Chiari, M.; Garcia-Orellana, I.; Lucarelli, F.; Migliori, A.; Nava, S.; Taccetti, F. The new external beam facility for environmental studies at the Tandetron accelerator of LABEC. *Nucl. Instrum. Methods B* **2006**, *249*, 928. [CrossRef]
21. Alberti, R.; Bjeoumikhov, A.; Grassi, N.; Guazzoni, C.; Klatka, T.; Longoni, A.; Quattrone, A. Use of silicon drift detectors for the detection of medium-light elements in PIXE. *Nucl. Instrum. Methods B* **2008**, *266*, 2296. [CrossRef]
22. Harrison, J.; Eldred, R. Automatic Data Acquisition and Reduction for Elemental Analysis of Aerosol Samples. *Adv. X-ray Anal.* **1973**, *17*, 560. [CrossRef]
23. Gatti, E.; Rehak, P. Semiconductor drift chamber—An application of a novel charge transport scheme. *Nucl. Instrum. Methods A* **1984**, *225*, 608. [CrossRef]
24. Orlic, I.; Zhou, S.; Sanchez, J.; Watt, F.; Tang, S. Virtual PIXE and RBS laboratory. *Nucl. Instrum. Methods B* **1999**, *150*, 83. [CrossRef]
25. Pichon, L.; Moignard, B.; Lemasson, Q.; Pacheco, C.; Walter, P. Development of a multi-detector and a systematic imaging system on the AGLAE external beam. *Nucl. Instrum. Methods B* **2014**, *318*, 27. [CrossRef]
26. Chiari, M.; Barone, S.; Bombini, A.; Calzolai, G.; Carraresi, L.; Castelli, L.; Czelusniak, C.; Fedi, M.; Gelli, N.; Giambi, F.; et al. LABEC, the INFN ion beam laboratory of nuclear techniques for environment and cultural heritage. *Eur. Phys. J. Plus* **2021**, *136*, 472. [CrossRef]
27. Šmit, Ž.; Uršič, M.; Pelicon, P.; Trček-Pečak, T.; Šeme, B.; Smrekar, A.; Langus, I.; Nemec, I.; Kavkler, K. Concentration profiles in paint layers studied by differential PIXE. *Nucl. Instrum. Methods B* **2008**, *266*, 2047. [CrossRef]
28. Enguita, O.; Climent-Font, A.; Garcia, G.; Montero, I.; Fedi, M.; Chiari, M.; Lucarelli, F. Characterization of metal threads using differential PIXE analysis. *Nucl. Instrum. Methods B* **2002**, *189*, 328. [CrossRef]
29. Barradas, N.P.; Cruz, J.; Fonseca, M.; Jesus, A.; Lagoyannis, A.; Manteigas, V.; Mayer, M.; Preketes-Sigalas, K.; Dimitriou, P. International Atomic Energy Agency inter-comparison of Particle Induced Gamma-ray Emission codes for bulk samples. *Nucl. Instrum. Methods B* **2020**, *468*, 37. [CrossRef]
30. Manteigas, V.; Martins, L.; Cruz, J.; Fonseca, M.; Jesus, A. ERYA-Bulk and ERYA-Profiling: An application for quantitative PIGE analysis. *Comput. Phys. Commun.* **2022**, *275*, 108307. [CrossRef]
31. Upp, D.L.; Keyser, R.M.; Twomey, T.R. New cooling methods for HPGE detectors and associated electronics. *JRNC* **2005**, *264*, 121. [CrossRef]

32. Grassi, N.; Migliori, A.; Mandò, P.; Calvo-del Castillo, H. Identification of lapis-lazuli pigments in paint layers by PIGE measurements. *Nucl. Instrum. Methods B* **2004**, *219–220*, 48. [CrossRef]
33. Grassi, N.; Giuntini, L.; Mandò, P.; Massi, M. Advantages of scanning-mode ion beam analysis for the study of Cultural Heritage. *Nucl. Instrum. Methods B* **2007**, *256*, 712. [CrossRef]
34. Climent-Font, A.; Munoz-Martin, A.; Ynsa, M.; Zucchiatti, A. Quantification of Sodium in Ancient Roman Glasses with Ion Beam Analysis. *Nucl. Instrum. Methods B* **2008**, *266*, 640. [CrossRef]
35. Abriola, D.; Barradas, N.; Bogdanović-Radović, I.; Chiari, M.; Gurbich, A.; Jeynes, C.; Kokkoris, M.; Mayer, M.; Ramos, A.; Shi, L.; et al. Development of a reference database for Ion Beam Analysis and future perspectives. *Nucl. Instrum. Methods B* **2011**, *269*, 2972. [CrossRef]
36. Gurbich, A. SigmaCalc recent development and present status of the evaluated cross-sections for IBA. *Nucl. Instrum. Methods B* **2016**, *371*, 27. [CrossRef]
37. Mayer, M. SIMNRA, a Simulation Program for the Analysis of NRA, RBS and ERDA. *AIP Conf Proc.* **1999**, *475*, 541.
38. Vadrucci, M.; Mazzinghi, A.; Sorrentino, B.; Falzone, S.; Gioia, C.; Loreti, E.; Chiari, M. Characterisation of ancient Roman wall-painting fragments using non-destructive IBA and MA-XRF techniques. *X-ray Spectrom.* **2020**, *49*, 668. [CrossRef]
39. Beck, L.; Jeynes, C.; Barradas, N. Characterization of paint layers by simultaneous self-consistent fitting of RBS/PIXE spectra using simulated annealing. *Nucl. Instrum. Methods B* **2008**, *266*, 1871. [CrossRef]
40. Jeynes, C.; Bailey, M.; Bright, N.; Christopher, M.; Grime, G.; Jones, B.; Palitsin, V.; Webb, R. "Total IBA"—Where are we? *Nucl. Instrum. Methods B* **2012**, *271*, 107. [CrossRef]
41. Calligaro, T.; Banas, A.; Banas, K.; Bogdanović-Radović, I.; Brajković, M.; Chiari, M.; Forss, A.; Hajdas, I.; Krmpotić, M.; Mazzinghi, A.; et al. Emerging nuclear methods for historical painting authentication: AMS-14C dating, MeV-SIMS and O-PTIR imaging, global IBA, differential- PIXE and full-field PIXE mapping. *Forensic Sci. Int.* **2022**, *336*, 111327. [CrossRef]
42. Barradas, N.; Jeynes, C.; Webb, R. Simulated annealing analysis of Rutherford backscattering data. *Appl. Phys. Lett.* **1997**, *71*, 291. [CrossRef]
43. Jeynes, C.; Palitsin, V.; Grime, G.; Pascual-Izarra, C.; Taborda, A.; Reis, M.; Barradas, N. External beam Total-IBA using DataFurnace. *Nucl. Instrum. Methods B* **2020**, *481*, 47. [CrossRef]
44. Calligaro, T.; Dran, J.-C.; Ioannidou, E.; Moignard, B.; Pichon, L.; Salomon, J. Development of an external beam nuclear microprobe on the Aglae facility of the Louvre museum. *Nucl. Instrum. Methods B* **2000**, *161–163*, 328. [CrossRef]
45. Calzolai, G.; Chiari, M.; Lucarelli, F.; Nava, S.; Portarena, S. Proton induced g-ray emission yields for the analysis of light elements in aerosol samples in an external beam set-up. *Nucl. Instrum. Methods B* **2010**, *268*, 1540. [CrossRef]
46. Isaković, K.; Petric, M.; Rupnik, Z.; Šmit, Ž.; Pelicon, P.; Kelemen, M.; Vereš, M.; Pongrac, P.; Vavpetič, P.; Kavčič, M. Upgrade of the external beamline at the microanalytical center of the Jožef Stefan Institute. *Nucl. Instrum. Methods B* **2022**, *510*, 69. [CrossRef]
47. Chiari, M.; Migliori, A.; Mandò, P. Measurement of low currents in an external beam set-up. *Nucl. Instrum. Methods B* **2002**, *188*, 162. [CrossRef]
48. Anttila, A.; Räisänen, J.; Lappalainen, R. On the optimization of an external PIXE arrangement. *Nucl. Instrum. Methods B* **1985**, *12*, 245. [CrossRef]
49. Mazzinghi, A.; Ruberto, C.; Castelli, L.; Ricciardi, P.; Czelusniak, C.; Giuntini, L.; Mandò, P.; Manetti, M.; Palla, L.; Taccetti, F. The importance of being little: MA-XRF on manuscripts on a Venetian island. *X-ray Spectr.* **2021**, *50*, 272. [CrossRef]
50. Mathot, S.; Anelli, G.; Atieh, S.; Bilton, A.; Bulat, B.; Callamand, T.; Calvo, S.; Favre, G.; Geisser, J.-M.; Gerardin, A.; et al. The CERN PIXE-RFQ, a transportable proton accelerator for the machina project. *Nucl. Instrum. Methods B* **2019**, *459*, 153. [CrossRef]